Wind and Structures, *Vol. 30, No. 5 (2020) 485-497*
DOI: https://doi.org/10.12989/was.2020.30.5.485

Hydrodynamic forces on blocks and vertical wall on a step bottom

Ramnarayan Mondal[1a] and Md. Mahbub Alam[*1,2]

[1]*Institute for Turbulence-Noise-Vibration Interaction and Control Harbin Institute of Technology, Shenzhen 518055, China*
[2]*Digital Engineering Laboratory of Offshore Equipment, Shenzhen, China*

(*Received September 12, 2019, Revised January 22, 2020, Accepted January 26, 2020*)

Abstract. A study, using potential water wave theory, is conducted on the oblique water wave motion over two fixed submerged rectangular blocks (breakwaters) placed over a finite step bottom. We have considered infinite and semi-infinite fluid domains. In both domains, the Fourier expansion method is employed to obtain the velocity potentials explicitly in terms of the infinite Fourier series. The unknown coefficients appearing in the velocity potentials are determined by the eigenfunction expansion matching method at the interfaces. The derived velocity potentials are used to compute the hydrodynamic horizontal and vertical forces acting on the submerged blocks for different values of block thickness, gap spacing between the two blocks, and submergence depth of the upper block from the mean free surface. In addition, the wave load on the vertical wall is computed in the case of the semi-infinite fluid domain for different values of blocks width and the incident wave angle. It is observed that the amplitudes of hydrodynamic forces are negligible for larger values of the wavenumber. Furthermore, the upper block experiences a higher hydrodynamic force than the lower block, regardless of the gap spacing, submergence depth, and block thickness.

Keywords: submerged breakwaters; uneven bottom; semi-infinite fluid domain

1. Introduction

In coastal engineering, submerged structures are used as breakwaters to protect the coastline and coastal structures from high wave attack. These breakwaters are environment-friendly as allowing water exchange between the sea and lee sides of those. Furthermore, their installation does not depend on the seabed condition as they can be easily installed or removed from the site, keeping a less footprint on the sea bed. In addition, they are economical compared with the traditional bottom-mounted breakwaters. In the marine environment, the other applications of submerged structures are artificial reefs, observatories, and submerged tunnels (Chakrabarti *et al*. 2008, Huang *et al*. 2016).

A number of studies (Patarapanich 1984, Patarapanich and Cheong 1989, Liu and Iskandarani 1991, Porter 2015, Behera and Sahoo 2015) have been carried out on the wave interaction with a thin horizontal submerged plate that is used to attenuate the wave height in the coastal region. Using potential water wave theory, they solved this problem and computed the reflected and transmitted wave energy to show the efficiency of a submerged plate as a breakwater. On the other hand, Wang and Shen (1999) using linear potential theory computed wave reflection and transmission by a group of submerged plates which are placed horizontally on a vertical line. They observed that the reflection and transmission coefficients depend on the plate length and the depth of the plates from the free water surface. The wave transmission decreases with the increase in the length of the plates. Mondal and Banerjea (2016) considered an inclined submerged porous plate in the ocean in the presence of an ice-covered surface and investigated the wave energy attenuation. They presented the reflection and transmission coefficients computed numerically for different physical parameters. They observed that due to the presence of inclined submerged plate, the reflection and transmission wave energy reduces.

In the above-mentioned studies, the plate thickness was not considered in the formulation of the problem. However, many researchers (Kojima *et al*. 1994, Cheong *et al*. 1996, Williams and McDougal 1996, Hu *et al*. 2002, Rahman *et al*. 2006, Zheng *et al*. 2007a, Peng *et al*. 2013) investigated the problem of water wave scattering by submerged rectangular blocks of finite thickness. Cheong *et al*. (1996) solved the problem of wave interaction with a fixed submerged body using eigenfunction expansion method (EEM) and finite element method (FEM). They numerically computed the reflection, transmission coefficients, and hydrodynamic forces acting on the submerged body. They observed that the EEM has a good agreement with FEM. Williams and McDougal (1996) adopted eigenfunction expansion technique and solved the problem of wave interaction with submerged structure. The derived solution was used to compute hydrodynamic force, added mass, reflection, and transmission coefficients. Furthermore, the computed results were compared with the results obtained from the model test and reasonable agreement was exhibited. The minimum transmission occurred near the surge natural frequency, with the radiated and diffracted waves having the same amplitudes in 180o phase. Zheng *et*

*Corresponding author, Professor
E-mail: alamm28@yahoo.com, alam@hit.edu.cn
[a]Ph.D. Postdoctoral fellow,
E-mail: ramju08@yahoo.com

ISSN: 1226-6116 (Print), 1598-6225 (Online)

al. (2007a) solved the problem of oblique wave scattering by an infinitely long rectangular submerged structure, using the variable separation and eigenfunction expansion matching methods. They presented numerical results for reflection and transmission coefficients, and hydrodynamic forces acting on the submerged body. Zheng *et al*. (2007b) studied the radiation and diffraction of linear water waves by a submerged structure in the presence of a vertical wall. They estimated the hydrodynamic forces acting on the submerged body and vertical wall. The hydrodynamic forces acting on the submerged body were periodic in nature, and the amplitude of forces decreased with the increase of the wavenumber and submergence depth.

In the aforementioned studies, a single submerged block was considered to investigate the problem of wave structure interaction. To the authors' knowledge, a few studies (Liu *et al*. 2009, Medina-Rodriguez and Silva 2018) are found on the wave interaction with multiple submerged blocks. Liu *et al*. (2009) used the eigenfunction expansion method to investigate the hydrodynamic performance of two side-by-side submerged horizontal breakwaters of equal width but of different thicknesses. They identified that the spacing between the two breakwaters does not influence much on the reflection of water waves.

In the above studies, the water depth was considered uniform. However, submerged structures commonly are installed near the coastline where the water depth is not uniform in general. Therefore, it is required to study the hydrodynamic performance of submerged structures in the presence of an uneven bottom. For simplicity, we consider a step bottom in the present study. Furthermore, these breakwaters are commonly used to protect bottom-mounted coastal structures such as vertical wall, jetties or wharfs and continental shelves, behaving as a vertical wall. Therefore, in the present study a vertical wall is also considered.

Recently, Mondal and Takagi (2016, 2019) studied wave scattering by a fixed submerged body in infinite and semi-infinite fluid domains. They computed the hydrodynamic forces acting on the submerged body. They observed that the bottom effect needs not to be considered if h/H > 0.9, where h and H are the water depths in shallower and deeper regions, respectively. In addition, they computed the amplitude of free water surface elevation and observed that the wave amplitude in the lee side is smaller than that of the seaside of submerged breakwaters. Thus, the submerged breakwater can provide a relatively calm region on the lee side. In the present study, we extend the work of Mondal and Takagi (2019) by considering two identical submerged blocks in both cases of infinite and semi-infinite fluid domains. In the presence of two submerged blocks, the model configuration domain differs from the work of Mondal and Takagi (2019). It was not possible to compute the hydrodynamic behavior from Mondal and Takagi's (2019) work by induction. We thus need to solve the present problem separately to understand the hydrodynamic behavior in the presence of two submerged blocks. Our aim is to solve the problem analytically using the eigenfunction expansion method and to compute the hydrodynamic forces acting on the submerged blocks and vertical wall for different geometrical parameters. Like other coastal structures, submerged blocks are pile-supported and for simplicity the pile effect is not incorporated in this study. The present study is of application in the design of multiple submerged horizontal block-type breakwaters used for mitigating wave attacks and coastal morphology control (Yu 2002, Wang *et al*. 2006).

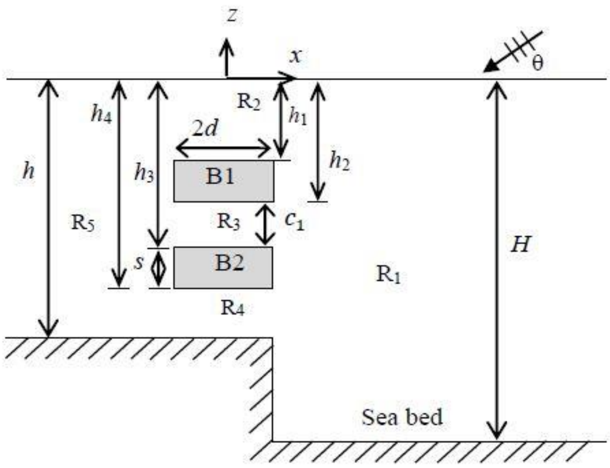

Fig. 1 Schematic view of submerged blocks and step bottom in infinite fluid domain

2. Problem statement and solution

The problem of wave interaction with two identical rectangular blocks fixed and submerged is studied for infinite and semi-infinite fluid domains under the assumption of small amplitude linear water wave theory. The problem statement and solution for infinite and semi-infinite cases are presented in subsequent subsections 2.1 and 2.2, respectively. In the present study, the three-dimensional Cartesian coordinate system is used such that the *x*-*y* plane represents mean free surface and the *z*-axis is vertically upward, with the origin located above the centers of the breakwaters (Fig. 1).

2.1. Infinite fluid domain

The side view of the submerged breakwaters (blocks), which are infinitely extended along the *y*-axis, in the infinite fluid domain is shown in Fig. 1. The two blocks (B1 and B2), each of width $2d$ and thickness s, are placed over the step at a depth h_1 and h_3, respectively, from the mean free surface. The gap spacing between the two breakwaters is denoted by $c_1 = h_3 - h_2$ (Fig. 1). At the seabed, a finite step at $x = d$ is considered, with the water depth changing from H to h ($< H$). Depending on the geometrical configuration, the fluid domain is divided into five regions, R_1: $d < x < \infty$, $-H < z < \eta$; R_2: $-d < x < d$, $-h_1 < z < \eta$; R_3: $-d < x < d$, $-h_3 < z < -h_2$; R_4: $-d < x < d$, $-h < z < -h_4$ and R_5: $-\infty < x < -d$, $-h < z < \eta$, where η is the free surface elevation from the mean water level.

The fluid of density ρ is considered inviscid, incompressible. The fluid motion is irrotational and simple harmonic in time, having angular frequency ω. Considering the small-amplitude water wave theory, the oblique water wave is adopted. It is also assumed that the incident waves propagate, making an angle θ with the positive x-axis. Thus, the velocity potential $\Phi(x,y,z,t)$ can be written as $\Phi(x,y,z,t) = \mathrm{Re}[\phi(x,z)e^{i(k_y y-\omega t)}]$, where Re represents the real part and $k_y = k_0 \sin\theta$ being the y-component of the incident wavenumber k_0. Therefore, the spatial velocity potential $\phi(x,z)$ satisfies the Helmholtz equation

$$\left(\frac{\partial^2}{\partial x^2}+\frac{\partial^2}{\partial z^2}-k_y^2\right)\phi = 0, \tag{1}$$

in the fluid domain.

Linearized free surface boundary condition at $z = 0$ is

$$\frac{\partial \phi}{\partial z}-\frac{\omega^2}{g}\phi = 0, \tag{2}$$

where g is the acceleration of gravity. As fluid does not penetrate through the seabed, the boundary conditions are as follows

$$\frac{\partial \phi}{\partial z} = 0, \text{ at } z = -H,\ d < x < \infty \text{ and } z = -h,\ -\infty < x < d \tag{3a}$$

$$\frac{\partial \phi}{\partial x} = 0, \text{ at } x = d,\ -H < z < -h. \tag{3b}$$

The boundary conditions on the rigid submerged breakwaters are prescribed as

$$\frac{\partial \phi}{\partial x} = 0, \text{ at } x = \pm d,\ h_{2j} < z < h_{2j-1}, \tag{4a}$$

$$\frac{\partial \phi}{\partial z} = 0, \text{ at z} = h_{2j-1}, h_{2j}\ \ -d < x < d, \tag{4b}$$

where $j = 1$ and 2 indicate the submerged blocks B1 and B2, respectively.

Along with the above boundary conditions, the velocity potential $\phi(x, z)$ satisfies the far-field radiation condition

$$\phi(x,z) \approx \left\{Ie^{-ik_{0x}(x-d)} + Re^{ik_{0x}(x-d)}\right\}\frac{\cosh k_0(H+z)}{\cosh k_0 H}, \text{ as } x \to \infty, \tag{5a}$$

$$\phi(x,z) \approx Te^{-i\kappa_{0x}(x+d)}\frac{\cosh \kappa_0(h+z)}{\cosh \kappa_0 h}, \text{ as } x \to -\infty, \tag{5b}$$

where I and R are associated with the incident and reflected wave heights, respectively, in region R_1, and T is associated with transmitted wave height in region R_5. The quantities $k_{0x} = k_0 \cos\theta$ and $\kappa_{0x} = \kappa_0 \cos\tilde{\theta}$ are the x-component of the incident wavenumber k_0 and transmitted wavenumber κ_0, respectively, where $\tilde{\theta}$ is the wave angle of the transmitted waves with the x- axis.

Using the eigenfunction expansion method, the velocity potentials $\phi(x, z)$ for each region R_l (where l = 1, 2, 3, 4 and 5) are computed. The velocity potentials $\phi_l(x, z)$ satisfy Eq. (1) along with the boundary conditions as in Eqs. (2) - (5). Proceeding in a similar manner as in Mondal and Takagi (2019), the velocity potentials $\phi_l(x, z)$ for each domain R_l are expressed as

$$\phi_1 = Ie^{-ik_{0x}(x-d)}f_0(z) + \sum_{n=0}^{\infty} A_n e^{ik_{nx}(x-d)}f_n(z), \tag{6}$$

$$\phi_2 = \sum_{n=0}^{\infty}\left(B_n\frac{\cos\mu_{nx}x}{\cos\mu_{nx}d} + C_n\frac{\sin\mu_{nx}x}{\sin\mu_{nx}d}\right)\psi_n(z), \tag{7}$$

$$\phi_3 = \sum_{n=0}^{\infty}\left(D_n\frac{\cosh p_{nx}x}{\cosh p_{nx}d} + E_n\frac{\sinh p_{nx}x}{\sinh p_{nx}d}\right)\varphi_n(z), \tag{8}$$

$$\phi_4 = \sum_{n=0}^{\infty}\left(F_n\frac{\cosh q_{nx}x}{\cosh q_{nx}d} + G_n\frac{\sinh q_{nx}x}{\sinh q_{nx}d}\right)\chi_n(z), \tag{9}$$

$$\phi_5 = H_0 e^{-i\kappa_{0x}(x+d)}g_0(z) + \sum_{n=1}^{\infty} H_n e^{\kappa_{nx}(x+d)}g_n(z), \tag{10}$$

where $\{X_n\} \equiv \{A_n, B_n, C_n, D_n, E_n, F_n, G_n, H_n\}$ are unknown constants to be determined to know the velocity potentials completely. The eigenfunctions $f_n(z)$, $\psi_n(z)$, $\varphi_n(z)$, $x_n(z)$ and $g_n(z)$ are given by

$$f_n(z) = \frac{\cosh k_n(H+z)}{\cosh k_n H}, \text{ for } n = 0, 1, 2, ..., \text{ and} \tag{11}$$

$$\varphi_n(z) = \begin{cases} 1, \text{ for } n = 0 \\ \cos p_n(h_3+z), \text{ for } n = 1, 2, ... \end{cases} \tag{12}$$

The eigenfunctions $\varphi_n(z)$ and $g_n(z)$ can be obtained from Eq. (11) replacing (k_n, H) by (μ_n, h_1) and (κ_n, h), respectively. In addition, the eigenfunction $\chi_n(z)$ as appearing in Eq. (9) can be obtained from Eq. (12) by replacing p_n and h_3 by q_n and h, respectively. The quantities, k_{nx}, μ_{nx}, p_{nx}, q_{nx} and κ_{nx}, which appear in Eqs. (6) - (10) are of the form

$$\begin{aligned} &k_{nx} = \sqrt{k_n^2 - k_y^2},\ \ p_{nx} = \sqrt{p_n^2 + k_y^2},\ \ q_{nx} = \sqrt{q_n^2 + k_y^2}, \\ &\mu_{nx} = \sqrt{\mu_n^2 - k_y^2},\ \ \kappa_{nx} = \sqrt{\kappa_n^2 - k_y^2}, \end{aligned} \tag{13}$$

With $p_n = n\pi/(h_3\text{-}h_2)$ and $p_n = n\pi/(h\text{-}h_4)$. The wavenumber $\lambda_n \equiv (k_n, \mu_n, \kappa_n)$ and associated water depth $\gamma = (H, h_1, h)$ satisfy the dispersion relation

$$\omega^2 = g\lambda_n \tanh \lambda_n\gamma,\ \ n = 0, 1, 2, ... \tag{14}$$

The eigenfunctions $f_n(z)$, $\psi_n(z)$ and $g_n(z)$ appearing in Eqs. (6), (7) and (10), respectively satisfy the following orthogonal relations

$$\int_{-H}^{0} f_m(z)f_n(z)dz = \mathscr{C}_n\delta_{mn}, \tag{15}$$

$$\int_{-H}^{0} f_m(z) f_n(z) dz = \mathscr{C}_n \delta_{mn}, \tag{15}$$

$$\int_{-h_1}^{0} \psi_m(z)\psi_n(z) dz = \mathscr{D}_n \delta_{mn} \quad \text{and} \tag{16}$$

$$\int_{-h}^{0} g_m(z) g_n(z) dz = \mathscr{H}_n \delta_{mn}, \tag{17}$$

for m, n = 0, 1, 2, …, and δ_{mn} is the Kronecker delta and the orthogonality constant $\mathscr{C}_n$ is of the form

$$\mathscr{C}_n = \frac{2k_n H + \sinh 2k_n H}{4k_n \cosh^2 k_n H}, \quad n = 0, 1, 2, \ldots. \tag{18}$$

The orthogonality constants D_n and H_n can be obtained from Eq. (18) replacing (k_n, H) by (μ_n, h_1) and (κ_n, h), respectively. On the other hand, the eigenfunctions $\varphi_n(z)$ and $\chi_n(z)$ appearing in Eqs. (8) and (9), respectively, satisfy the orthogonal relations

$$\int_{-h_3}^{-h_2} \varphi_m(z)\varphi_n(z) dz = \mathscr{Y}_n \delta_{mn}, \text{ and} \tag{19}$$

$$\int_{-h}^{-h_4} \chi_m(z)\chi_n(z) dz = \mathscr{X}_n \delta_{mn} \tag{20}$$

for m, n = 0, 1, 2, … and the orthogonality constant $\mathscr{Y}_n$ is of the form

$$\mathscr{Y}_n = \varepsilon_n h_3 \left(1 - \frac{h_2}{h_3}\right), \text{ n = 0, 1, 2,…} \tag{21}$$

where ε_n = 1 for n = 0, else ε_n = 1/2. The orthogonality constant $\mathscr{X}_n$ can be obtained from Eq. (21) by replacing h_2 and h_3 by h_4 and h, respectively.

For the computation of unknowns $\{X_n\}$, the continuities of velocity and pressure are introduced at the interfaces $x = \pm d$ in the following forms

$$\phi_1 = \phi_{1+l}, \quad \frac{\partial \phi_1}{\partial x} = \frac{\partial \phi_{1+l}}{\partial x}, \quad \text{and} \tag{22}$$

$$\phi_5 = \phi_{1+l}, \quad \frac{\partial \phi_5}{\partial x} = \frac{\partial \phi_{1+l}}{\partial x}, \tag{23}$$

where suffix l = 1, 2 and 3 are associated with the spacing $-h_1 < z < 0$, $-h_3 < z < -h_2$, and $-h < z < -h_4$, respectively. The matching conditions (Eqs. (22), (23)), boundary conditions (Eqs. (3b), (4a)), and the orthogonal relations (Eqs. (15) – (17), (19) – (20)) are used to obtain a system of algebraic equations of unknowns $\{X_n\}$ which appear in Eqs. (6) – (10).

First, we consider the matching conditions of pressure at $x = d$ as defined in Eqs. (22), and (23) along with the orthogonality relations of $\psi_n(z)$, $\varphi_n(z)$ and $\chi_n(z)$ as defined in Eqs. (16), (19) and (20), respectively, which yield the system of equations

$$\sum_{n=0}^{\infty} A_n \int_{-h_1}^{0} f_n(z)\psi_m(z) dz - (B_m + C_m)\mathscr{D}_m = -I \int_{-h_1}^{0} f_0(z)\psi_m(z) dz, \tag{24}$$

$$\sum_{n=0}^{\infty} A_n \int_{-h_3}^{-h_2} f_n(z)\varphi_m(z) dz - (D_m + E_m)\mathscr{Y}_m = -I \int_{-h_3}^{-h_2} f_0(z)\varphi_m(z) dz \tag{25}$$

$$\sum_{n=0}^{\infty} A_n \int_{-h}^{-h_4} f_n(z)\chi_m(z) dz - (F_m + G_m)\mathscr{X}_m = -I \int_{-h}^{h_4} f_0(z)\chi_m(z) dz \tag{26}$$

where m = 0, 1, 2, …. Again, considering the first relations of Eqs. (22) and (23) at $x = -d$ and applying the orthogonality relations of $\psi_n(z)$, $\varphi_n(z)$ and $\chi_n(z)$ as in Eqs. (16), (19) and (20), we obtain

$$(B_m - C_m)\mathscr{D}_m - \sum_{n=0}^{\infty} H_n \int_{-h_1}^{0} g_n(z)\psi_m(z) dz = 0, \tag{27}$$

$$(D_m - E_m)\mathscr{Y}_m - \sum_{n=0}^{\infty} H_n \int_{-h_3}^{-h_2} g_n(z)\varphi_m(z) dz = 0, \text{ and} \tag{28}$$

$$(F_m - G_m)\mathscr{X}_m - \sum_{n=0}^{\infty} H_n \int_{-h}^{-h_4} g_n(z)\chi_m(z) dz = 0, \tag{29}$$

where m = 0, 1, 2, …. The no flow boundary conditions (Eqs. 3b, 4a) and the continuity of velocity (Eq. 22) at $x = d$, along with the orthogonality relation of $f_n(z)$ (Eq. 15) yield

$$ik_{0x}\mathscr{C}_0(I - A_0) = J_0, \quad k_{mx}\mathscr{C}_m A_m = J_m, \tag{30}$$

where J_m is given by

$$\begin{aligned} J_m = {} & \sum_{n=0}^{\infty} \mu_{nx}(B_n \tan \mu_{nx} d - C_n \cot \mu_{nx} d) \int_{-h_1}^{0} \psi_n(z) f_m(z) dz \\ & - \sum_{n=0}^{\infty} p_{nx}(D_n \tanh p_{nx} d + E_n \coth p_{nx} d) \int_{-h_3}^{-h_2} \varphi_n(z) f_m(z) dz \\ & - \sum_{n=0}^{\infty} q_{nx}(F_n \tanh q_{nx} d + G_n \coth q_{nx} d) \int_{-h}^{-h_4} \chi_n(z) f_m(z) dz, \end{aligned} \tag{31}$$

for m = 0, 1, 2, …. Lastly, we consider the no-flow boundary condition (Eq. 4a), matching condition of velocity (Eq. (23)) at $x = -d$ and implement the orthogonality condition of $g_n(z)$ (Eq. 17) which give

$$J_0 = -i\kappa_{0x}\mathscr{H}_0 H_0, \quad J_m = \kappa_{mx}\mathscr{H}_m H_m, \tag{32}$$

where

$$\begin{aligned} J_m &= \sum_{n=0}^{\infty} \mu_{nx}(B_n \tan \mu_{nx} d + C_n \cot \mu_{nx} d) \int_{-h_1}^{0} \psi_n(z) g_m(z) dz \\ &-\sum_{n=0}^{\infty} p_{nx}(D_n \tanh p_{nx} d - E_n \coth p_{nx} d) \int_{-h_3}^{-h_2} \varphi_n(z) g_m(z) dz \\ &-\sum_{n=0}^{\infty} q_{nx}(F_n \tanh q_{nx} d - G_n \coth q_{nx} d) \int_{-h}^{-h_4} \chi_n(z) g_m(z) dz \end{aligned} \tag{33}$$

where m = 0, 1, 2,… Eqs. (24) - (30) and (32) represent a system of linear algebraic equations of unknowns $\{X_n\}$, n = 0, 1, 2,… which appear in velocity potentials ϕ_l, l = 1, 2, 3, 4 and 5. For the purpose of numerical computation, we need to truncate the infinite series over n for a large value of $n = N$ for which the infinite series converges. Suppose, the infinite series over A_n, B_n, C_n, D_n, E_n, F_n, G_n and H_n converge for n = N_1, N_2, N_3, N_4, N_5, N_6, N_7 and N_8, respectively. Therefore, Eqs. (24 – 30) and (32), yield $\sum_{j=1}^{8}(N_j+1)$ linear algebraic equations having the same number of unknowns. For the purpose of simplicity, we consider $N = \max\{N_1, N_2, \ldots, N_8\}$. This gives the total number of (8N+8) algebraic equations having the same number of unknowns. The solution of the above system of equations (Eqs. (24) – (30) and (32)) provides the velocity potentials completely.

2.2. Semi-infinite fluid domain

In the present subsection, we formulate and solve the problem of wave diffraction by two submerged breakwaters and a step bottom in the case of semi-infinite fluid domain. The geometrical configuration of the fluid domain and submerged blocks are considered the same as discussed in subsection 2.1, except a vertical rigid wall assumed at x = -L as in Fig. 2. Considering geometrical configuration, the semi-infinite fluid domain can be divided into five regions where regions R_1 – R_4 are the same as defined in the case of the infinite fluid domain. The region R_5 in the semi-infinite fluid domain is given by $-L < x < -d$, $-h < z < \eta$, where η is the free surface elevation from the mean water level. We assume that the fluid properties are the same as stated in subsection 2.1. Hence, the velocity potential ϕ satisfies the governing Eq. (1) along with the boundary conditions (Eqs. (2) – (5a)). In addition, no flux across rigid vertical wall yields

$$\frac{\partial \phi}{\partial x} = 0, \quad \text{at } x = -L, \ -h < z < \eta \tag{34}$$

Proceeding in a similar manner as stated in subsection 2.1, the velocity potentials are computed in the case of the semi-infinite fluid domain and the details are not given here to avoid repetition. It is observed that the velocity potentials ϕ_l, where l = 1, 2, 3 and 4 are associated with regions R_1, R_2, R_3 and R_4, respectively, are of the same form as defined in Eqs. (6) - (9). On the other hand, the velocity potential ϕ_5 in region R_5 is obtained as

$$\phi_5 = \sum_{n=0}^{\infty} H_n \frac{\cos \kappa_{nx}(L+x)}{\cos \kappa_{nx}(L-d)} g_n(z), \tag{35}$$

where H_n, n = 0, 1, 2, … are unknown constants. The eigenfunction $g_n(z)$ and eigenvalues κ_{nx} are of the same form as stated in sub-section 2.1. Considering the matching condition at $x = d$ as defined in Eqs. (22); boundary conditions (Eqs. 3b, 4a) and orthogonality properties of $f_n(z)$, $\psi_n(z)$, $\varphi_n(z)$ and $\chi_n(z)$ give the same set of algebraic equations as defined in Eqs. (24), (25), (26) and (30). Furthermore, using the first relation of Eq. (23) at x = – d along with the orthogonality relations of $\psi_n(z)$, $\varphi_n(z)$ and $\chi_n(z)$, we obtain the same set of algebraic equations as in Eqs. (27), (28) and (29). However, the second relation of Eq. (23), no flux boundary condition in Eq. (4a) at x = – d, and orthogonality relation of $g_n(z)$ Eq. (17) give the following system of equations

$$\begin{aligned} J_0 &= -H_0\{\kappa_{0x} \tan \kappa_{0x}(L-d)\mathscr{H}_m\}, \\ J_m &= -H_n\{\kappa_{nx} \tanh \kappa_{0x}(L-d)\mathscr{H}_m\}, \quad m = 0,1,2,... \end{aligned} \tag{36}$$

where $\tilde{J}_m$ is of the same form as defined in Eq. (33). As done in the case of the infinite fluid domain, in the semi-infinite fluid domain we solve the system of Eqs. (24) – (30) and (36) to find out the unknown constants $\{X_n\}$.

3. Results and discussion

In this section, hydrodynamic forces acting on the submerged blocks and vertical wall are discussed for different physical parameters. The horizontal force (F_{x1}, F_{x2}) and vertical force (F_{z1}, F_{z2}), where subscripts 1 and 2 represent the blocks B1 and B2, respectively, are computed by

$$F_{xj} = i\rho\omega \int_{-h_{2j}}^{-h_{2j-1}} \{\phi_1(d,z) - \phi_5(-d,z)\} dz, \quad j = 1, 2 \ \text{and} \tag{37}$$

$$F_{zj} = i\rho\omega \int_{-d}^{d} \{\phi_{j+1}(x, h_{2j-1}) - \phi_{j+2}(x, h_{2j})\} dx, \quad j = 1, 2. \tag{38}$$

The hydrodynamic force (F_{xw}) acting on the vertical wall at $x = -L$ is evaluated by

$$F_{xw} = i\rho\omega \int_{-h}^{0} \phi_5(-L,z) dz \tag{39}$$

The hydrodynamic forces and free surface elevation in the non-dimensional form are

$$F_{xj}^* = \frac{F_{xj}}{\rho g H \zeta_a}, \quad F_{zj}^* = \frac{F_{zj}}{\rho g H \zeta_a}, \quad F_{xw}^* = \frac{F_{xw}}{\rho g H \zeta_a}, \tag{40}$$

where j = 1, 2; and ζ_a is the incident wave amplitude. The

Table 1 Horizontal and vertical forces acting on block B1 in infinite fluid domain

N	Horizontal Force				Vertical Force			
	k_0H=0.5	k_0H =2.0	k_0H=4.0	k_0H=8.0	k_0H=0.5	k_0H=2.0	k_0H=4.0	k_0H=8.0
0	0.0400	0.0829	0.066	0.0266	0.0765	0.2956	0.1984	0.0867
5	0.0447	0.0967	0.0738	0.0272	0.0889	0.3749	0.2344	0.0923
10	0.0460	0.0989	0.0747	0.0260	0.0919	0.3824	0.2369	0.0924
20	0.0466	0.0998	0.0751	0.0255	0.0920	0.3827	0.2367	0.0923
40	0.0467	0.1000	0.0751	0.0253	0.0924	0.3845	0.2374	0.0925
60	0.0468	0.1000	0.0751	0.0253	0.0926	0.3849	0.2375	0.0925
80	0.0468	0.1001	0.0751	0.0253	0.0926	0.3849	0.2376	0.0926

Table 2 Horizontal and vertical forces acting on block B2 in infinite fluid domain

N	Horizontal Force				Vertical Force			
	k_0H=0.5	k_0H =2.0	k_0H=4.0	k_0H=8.0	k_0H=0.5	k_0H=2.0	k_0H=4.0	k_0H=8.0
0	0.0356	0.0512	0.0291	0.0031	0.0178	0.0839	0.0863	0.0086
5	0.0358	0.0551	0.0322	0.0028	0.0129	0.0945	0.0836	0.0032
10	0.0373	0.0567	0.0324	0.0021	0.0127	0.0981	0.0849	0.0038
20	0.0378	0.0574	0.0328	0.0019	0.0127	0.0977	0.0848	0.0035
40	0.0378	0.0575	0.0328	0.0019	0.0126	0.0983	0.0849	0.0036
60	0.0379	0.0576	0.0328	0.0019	0.0126	0.0985	0.0849	0.0036
80	0.0379	0.0576	0.0328	0.0019	0.0126	0.0985	0.0849	0.0037

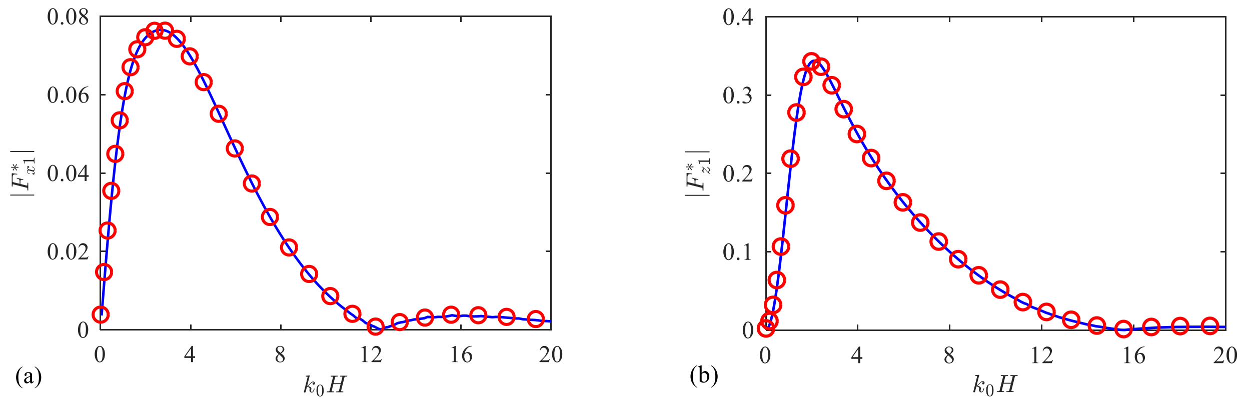

Fig. 3 Comparison of present result (blue line) with Mondal and Takagi's (2019) (red circles)

numerical results for the infinite and semi-infinite fluid domains are discussed in subsections 3.1 and 3.2, respectively.

3.1. Infinite fluid domain

In this section, the hydrodynamic wave forces acting on the submerged blocks are computed which can be used for the modeling of submerged breakwaters, reefs, observatories and submerged tunnels. In Section 2, we have stated that the infinite series appearing in Eqs. (6) - (10) are truncated at $n = N$. Therefore, before doing extensive numerical computations, it is required to find the minimum value of N for which the numerical results converge. Here, we find out the minimum value of N numerically. To examine the convergence, the horizontal and vertical forces acting on the submerged blocks B1 and B2 are computed for different values of k_0H = 0.5, 2, 4 and 8, and N = 0, 5, 10, 20, 40, 60 and 80 where the values of different geometrical parameters are chosen as h/H = 0.75, h_1/H = 0.2, h_3/H = 0.5, s/H = 0.1, d/H = 0.25, and θ = 30°. In all other numerical computations, we considered the above numerical values of geometrical parameters unless it is mentioned. The horizontal and vertical forces acting on the blocks B1 and B2 are presented in Table 1 and Table 2, respectively. From Tables 1 and 2, it is observed that in all the cases, the hydrodynamic forces acting on the submerged blocks are correct up to three decimal places for N = 40, 60 and 80. Therefore, N = 40 is adequate for the purpose of numerical computation which gives 328 linear algebraic equations having the same number of unknowns. These equations are solved to compute hydrodynamic forces which are presented in Figs. 3 - 6.

Furthermore, to show the accuracy of the present computation, we compare the present result with the computed result of Mondal and Takagi (2019). They considered the problem of water wave scattering by a fixed submerged block in the presence of a step bottom. Presently, the thickness s/H of block B2 and gap spacing c_2/H,(c_2 = h - h_4) cannot be set to zero. Therefore, we considered a sufficiently small value of s/H = 0.0001 (for block B2) and c_2/H = 0.0001. In Fig. 3, the horizontal and

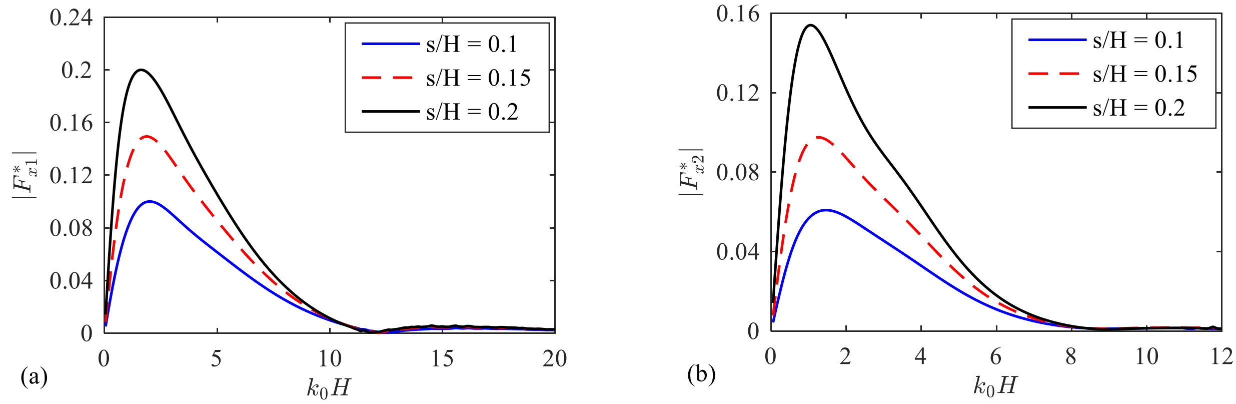

Fig. 4 Variations in horizontal forces on blocks (a) B1 and (b) B2 with k_0H for different values of thickness s/H. $h_1/H = 0.2$; $h_3/H = 0.5$

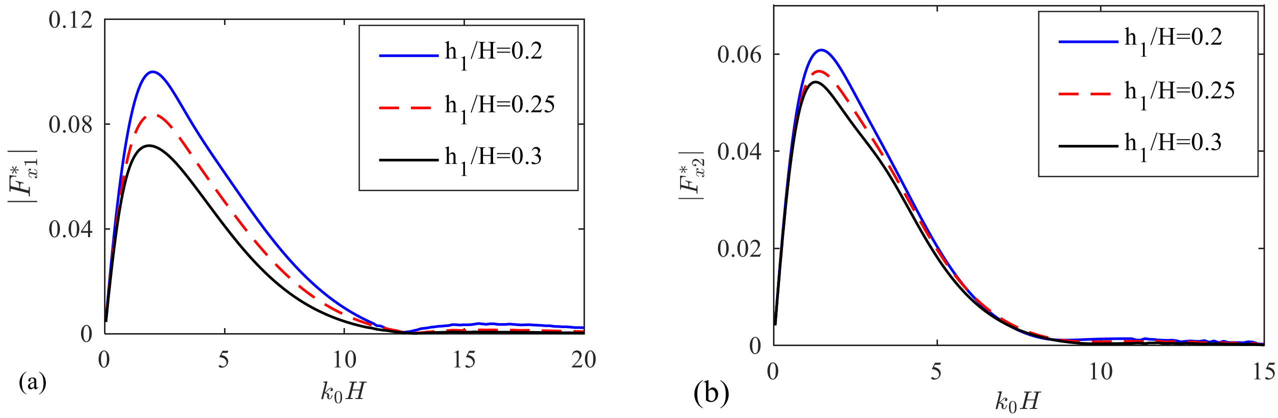

Fig. 5 Variations in horizontal forces on blocks (a) B1 and (b) B2 with k_0H for different values of submergence depth h_1/H of the upper block B1. $h_3/H = 0.5$; $s/H = 0.1$

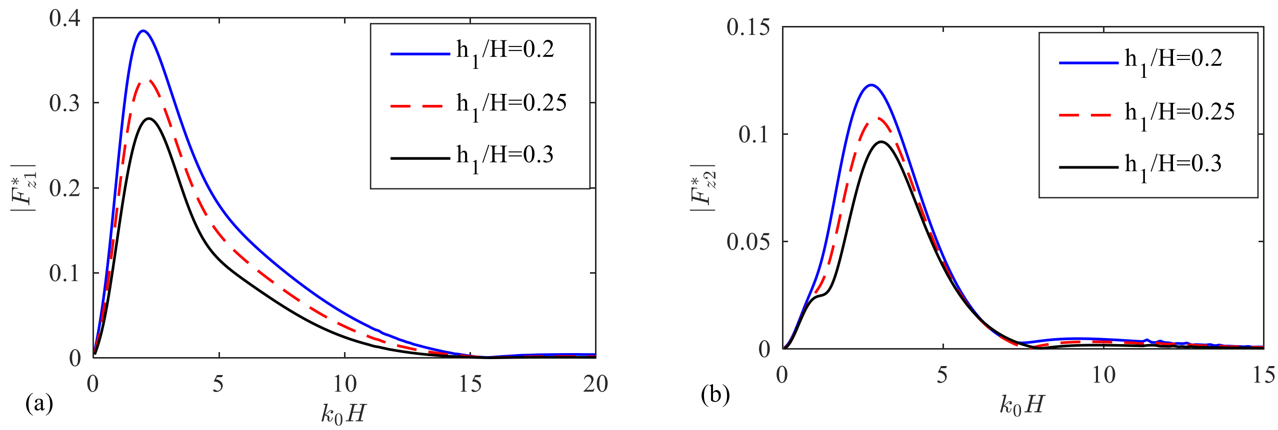

Fig. 6 Variations in vertical forces on blocks (a) B1 and (b) B2 with k_0H for different values of submergence depth h_1/H of the upper block B1. $h_3/H = 0.5$; $s/H = 0.1$

vertical forces acting on the block B1 are plotted against k_0H with $h_1/H = 0.2$ and $s/H = 0.1$, thickness of block B1. Fig. 3 depicts that both the horizontal and vertical forces computed from the present case (blue line) have a good agreement with those computed by Mondal and Takagi (2019) (red circle) which illustrate the accuracy of the present computation.

In Fig. 4, hydrodynamic horizontal forces acting on the submerged blocks B1 and B2 are plotted as functions of non-dimensional wavenumber k_0H for different values of block thickness s/H (= 0.1, 0.15, and 0.2), with $h_1/H = 0.2$ and $h_3/H = 0.5$. Fig. 4 shows that, with the increase of k_0H, the forces initially grow and reach maxima before progressively declining to zero. The maximum force on body B1 occurs at $k_0H = 2.0$, 1.86 and 1.63 for the thickness $s/H = 0.1$, 0.15 and 0.2, respectively, whereas that on body

Table 3 Horizontal and vertical forces acting on block B1 in semi-infinite fluid domain

N	Horizontal Force				Vertical Force			
	k_0H=0.5	k_0H =2.0	k_0H=4.0	k_0H=8.0	k_0H=0.5	k_0H=2.0	k_0H=4.0	k_0H=8.0
0	0.0431	0.1438	0.0673	0.0367	0.1856	0.0338	0.2130	0.1202
5	0.0553	0.1647	0.0819	0.0355	0.2490	0.0038	0.3050	0.1455
10	0.0576	0.1663	0.0868	0.0348	0.2525	0.0030	0.3106	0.1455
20	0.0580	0.1679	0.0896	0.0349	0.2529	0.0038	0.3164	0.1459
40	0.0583	0.1680	0.0905	0.0348	0.2541	0.0045	0.3199	0.1459
60	0.0583	0.1680	0.0908	0.0348	0.2545	0.0047	0.3199	0.1459
80	0.0584	0.1681	0.0909	0.0348	0.2546	0.0048	0.3199	0.1459

Table 4 Horizontal and vertical forces acting on block B2 in semi-infinite fluid domain

N	Horizontal Force				Vertical Force			
	k_0H=0.5	k_0H =2.0	k_0H=4.0	k_0H=8.0	k_0H=0.5	k_0H=2.0	k_0H=4.0	k_0H=8.0
0	0.0443	0.1112	0.0357	0.0056	0.0724	0.3980	0.1135	0.0096
5	0.0589	0.1236	0.0343	0.0036	0.1268	0.4356	0.0244	0.0201
10	0.0598	0.1271	0.0340	0.0038	0.1263	0.4421	0.0249	0.0207
20	0.0601	0.1271	0.0331	0.0034	0.1265	0.4430	0.0192	0.0214
40	0.0603	0.1272	0.0327	0.0033	0.1272	0.4440	0.0159	0.0214
60	0.0604	0.1272	0.0325	0.0033	0.1275	0.4441	0.0152	0.0214
80	0.0604	0.1272	0.0325	0.0033	0.1275	0.4441	0.0150	0.0214

B2 prevails at k_0H = 1.47, 1.25 and 1.06. That is, the k_0H corresponding to the maximum force is inversely related to s/H. The force on the submerged body increases with the increase of the thickness because the frontal surface area increases with the increase of thickness. In the case of the upper body B1, the force tends to zero at $k_0H \approx 11$, whereas in the case of lower body B2, the force becomes zero for smaller values of $k_0H \approx 8.5$. Furthermore, for a given s/H, the upper body undergoes more force than the lower body (Fig. 4a, b). This happens as the hydrodynamic pressure decrease with the increase in the water depth. We observed that the thickness had a negligible effect on the vertical component of hydrodynamic force acting on the submerged blocks B1 and B2 (results are not shown here).

Variations in the horizontal hydrodynamic force acting on blocks B1 and B2 with k_0H are presented in Fig. 5 for three different values of submergence depth of block B1 (h_1/H = 0.2, 0.25 and 0.3) when h_3/H = 0.5 and s/H = 0.1. For the same initial conditions (e.g. h_3/H = 0.5 and s/H = 0.1), the vertical forces acting on blocks B1 and B2 are computed as presented in Fig. 6. Both horizontal and vertical forces escalate with the increasing k_0H up to k_0H = 1.39 – 3.08 (depending on h_1/H) and drop with a further increase in k_0H. The horizontal and vertical forces on block B1 become negligible for $k_0H \geq 12.6$ and $k_0H \geq 15$, respectively. However, the forces acting on block B2 tend to zero for smaller values of $k_0H \geq 10$ (horizontal force) and $k_0H \geq 7.78$ (vertical force). The horizontal and vertical forces acting on block B1 is always greater than those acting on block B2. Furthermore, the forces decrease with the increase in the submergence depth of block B1.

3.2 Semi-infinite fluid domain

In this subsection, the results associated with the semi-infinite fluid domain are discussed. For the semi-infinite fluid domain, we need to find out the minimum value of N for which numerical results converge. For the numerical computation of hydrodynamic forces, the vertical wall is assumed at a distance L/H = 1.0 and the values of other parameters are assumed the same as adopted for the infinite fluid domain under subsection 3.1. To check the convergence numerically, the hydrodynamic horizontal and vertical forces on blocks B1 and B2 are calculated for four different values of k_0H = 0.5, 2, 4 and 8, and N = 0, 5, 10, 20, 40, 60 and 80. The magnitudes of forces acting on blocks B1 and B2 are tabulated in Tables 3 and 4, respectively. The forces are correct up to three decimal places for $N \geq 40$. This value is the same as obtained in the case of the infinite fluid domain. Thus, N = 40 is adequate for numerical computation.

In support of the present computation, for the limiting case, we compare the results computed from the present solution with the result of Mondal and Takagi (2019) who considered the problem of wave scattering by a submerged block in the semi-infinite fluid domain (Fig. 7). As stated in subsection 3.1, we cannot consider zero thickness of block B2. Therefore, as a limiting case we substitute s/H = 0.0001 (for block B2) and c_2/H = 0.0001, which are the same considered in the infinite fluid domain (subsection 3.1). The numerical values of the other geometrical parameters are h/H =0.75, h_1/H = 0.25, s/H = 0.2, L/H = 1.0 and θ = 30°. From Fig. 7, it is observed that both results agree well with each other. This shows the efficiency of the present solution

In the semi-infinite fluid domain, the hydrodynamic horizontal and vertical forces acting on the submerged blocks B1 and B2 are shown in Figs. 8 - 13, whereas Figs. 14, 15 and 16 present the hydrodynamic force acting on the vertical wall. Fig. 8 displays the horizontal forces acting on blocks B1 and B2 as functions of k_0H for s/H = 0.1, 0.15, and 0.2, where blocks B1 and B2 are considered at depths h_1/H = 0.2 and h_3/H = 0.5, respectively. For the same configurations, the vertical forces are presented in Fig. 9. Interestingly, the dependence of the forces on k_0H in the

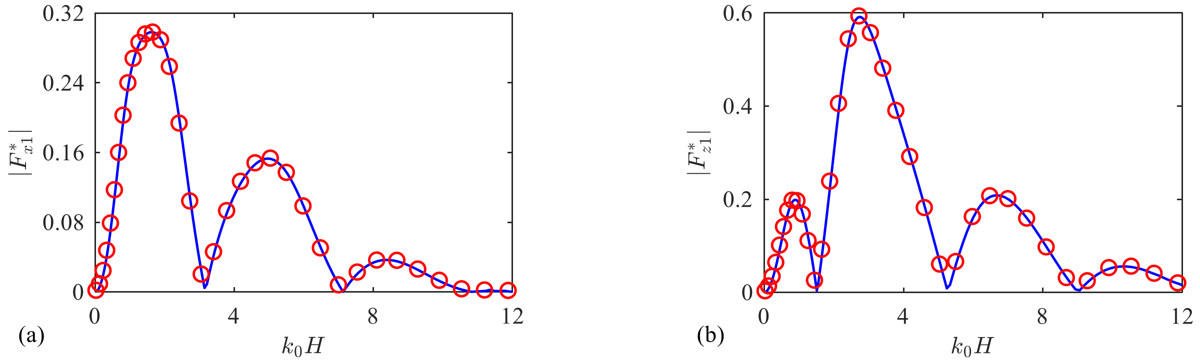

Fig. 7 Comparison of present result (blue line) with Mondal and Takagi's (2019) (red circles)

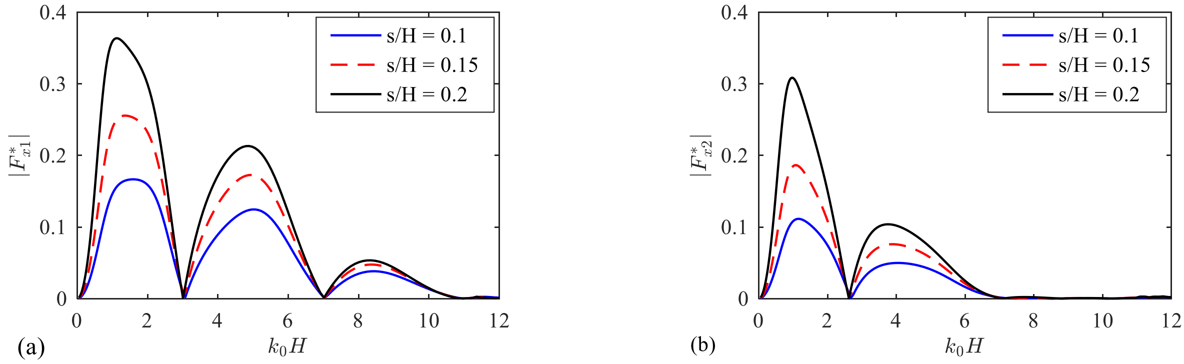

Fig. 8 Variation of horizontal force on blocks (a) B1 and (b) B2 with k_0H for different values of thickness s/H. $h_1/H = 0.2$; $h_3/H = 0.5$

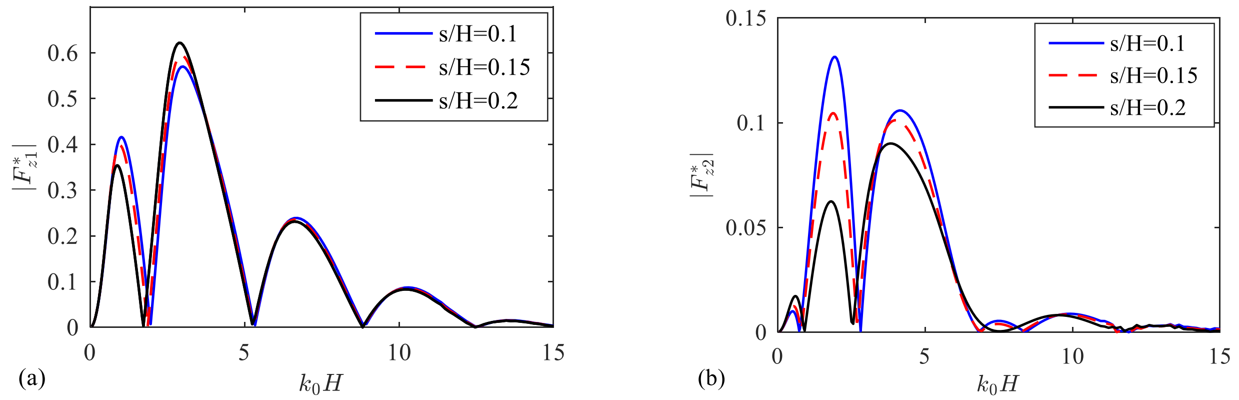

Fig. 9 Variation of vertical force on blocks (a) B1 and (b) B2 with k_0H for different values of thickness s/H. $h_1/H = 0.2$; $h_3/H = 0$

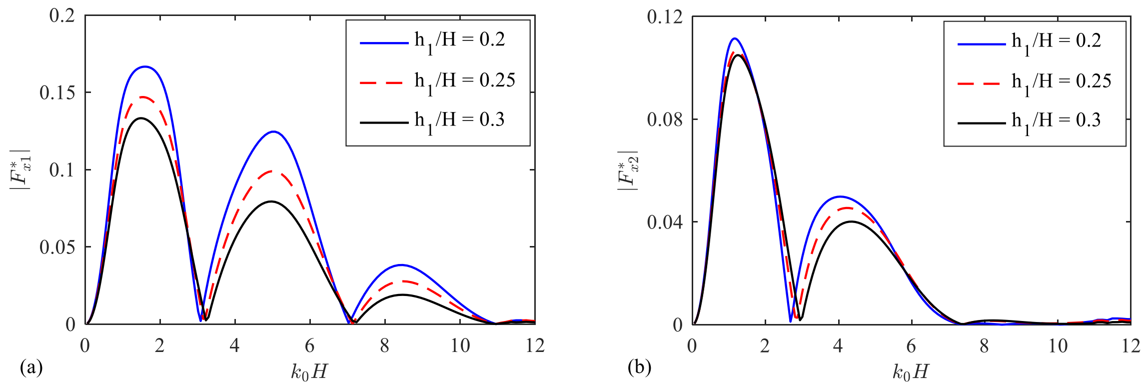

Fig. 10 Variation of horizontal force on blocks (a) B1 and (b) B2 with k_0H for different values of h_1/H. $h_3/H = 0.5$; $s/H = 0.1$

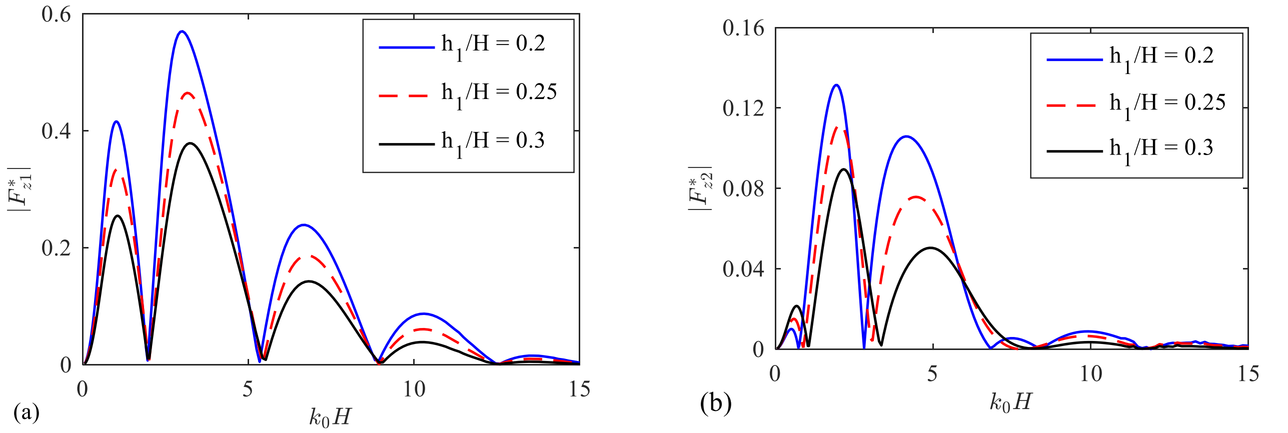

Fig. 11 Variation of vertical force on blocks (a) B1 and (b) B2 with k_0H for different values of h_1/H. $h_3/H = 0.5$; $s/H = 0.1$

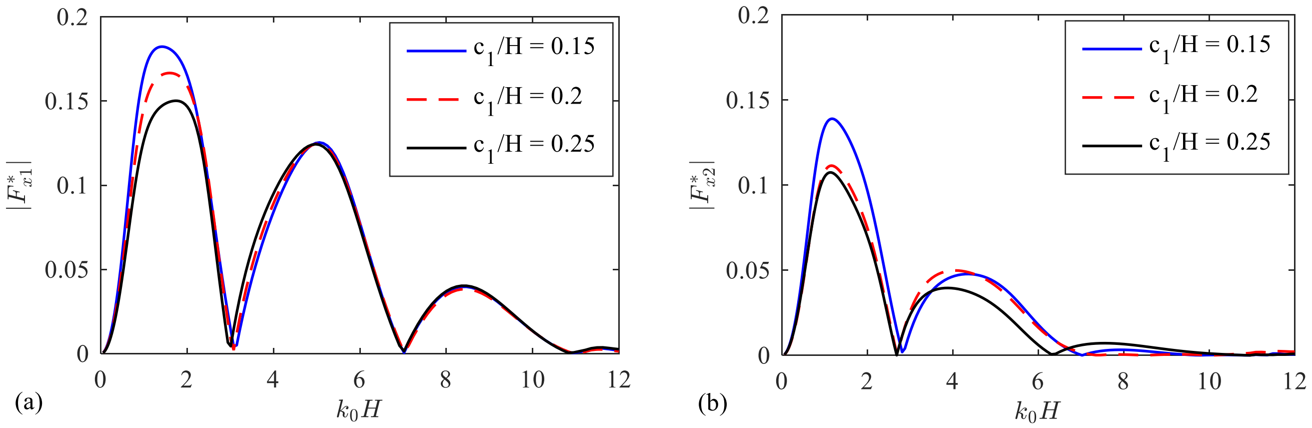

Fig. 12 Variation of horizontal force on blocks (a) B1 and (b) B2 with k_0H for different values of gap spacing c_1/H. $h_1/H = 0.2$; $h_3/H = 0.5$; $s/H = 0.1$

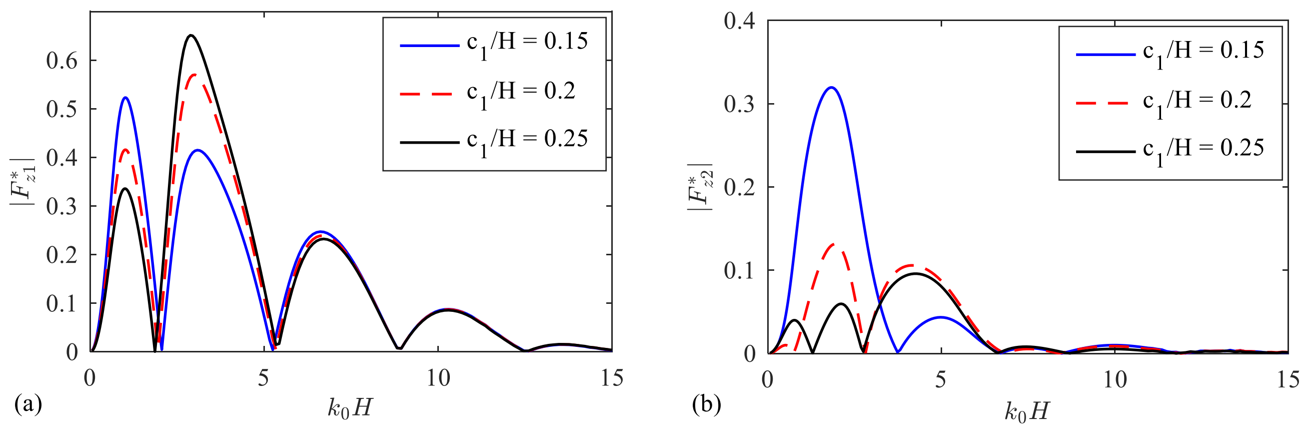

Fig. 13 Variation of vertical force on blocks (a) B1 and (b) B2 with k_0H for different values of gap spacing c_1/H. $h_1/H = 0.2$; $h_3/H = 0.5$; $s/H = 0.1$

semi-infinite domain is different from that in the infinite domain (Figs. 4, 8, 9). The horizontal forces increase and decrease in a damped wavy pattern (Figs. 8 and 9). It is expected that minimum and maximum values occur repeatedly owing to the interaction of incident waves and reflected waves from the vertical wall. The horizontal force on block B1 is negligible for $k_0H > 11$. This value is the same as obtained in the infinite fluid domain. However, it is smaller ($k_0H > 7$) for block B2. The horizontal force on block B1 is zero at $k_0H = 0.01$, 3.01, and 7.02, irrespective of s/H. Obviously, the periodicity of the force to be zero is not constant, but longer at higher k_0H. Similarly, the horizontal force on block B2 is zero at $k_0H = 0.01$, 2.62 and 7.25. The peak magnitude of the force increases with the

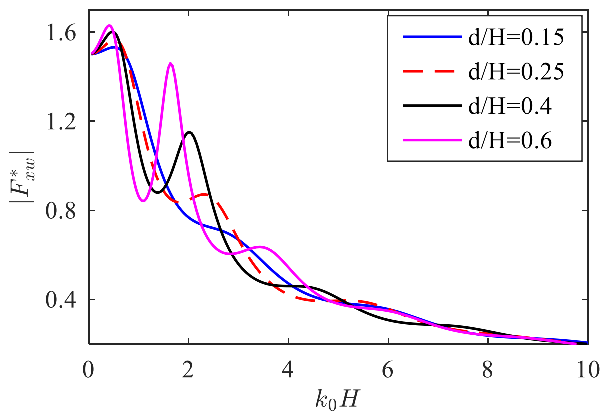

Fig. 14 Non-dimensional hydrodynamic force on vertical wall for different values of *d/H* as a function of k_0H where $L/H = 1.0$ and $\theta = 30^o$

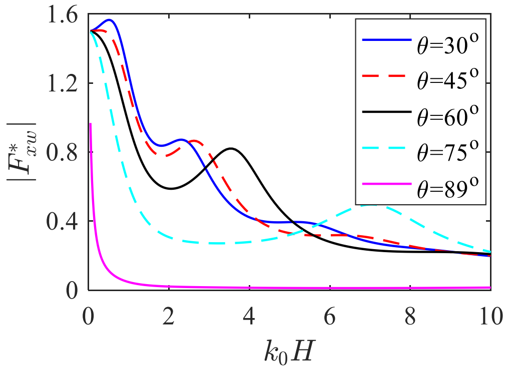

Fig. 15 Force on the vertical wall for different values of incident angle θ. $h_1/H = 0.2$, $h_3/H = 0.5$, $s/H = 0.1$, and $L/H = 1.0$

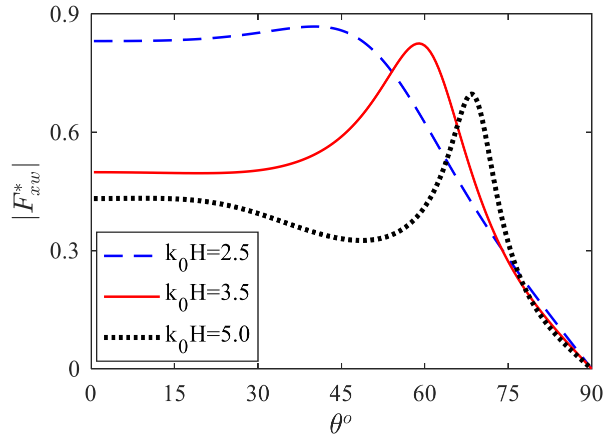

Fig. 16 Force on the vertical wall versus incident wave angle θ for different values of k_0H with $h_1/H = 0.2$, $h_3/H = 0.5$, $s/H = 0.1$, and $L/H = 1.0$

increase in *s/H*, as expected. On the other hand, the vertical force on B1 is not appreciably sensitive to *s/H* (Fig. 9a). However, *s/H* has a considerable effect on vertical force on block B2.

Figs. 10 and 11 show the variations in the horizontal and vertical forces with k_0H for $h_1/H = 0.2$, 0.25 and 0.3, with $h_3/H = 0.5$ and $s/H = 0.1$. The horizontal force on block B1 increases with k_0H for $k_0H = 0.1 – 1.5$. Reaching a maximum at $k_0H = 1.5$, it declines with further increasing k_0H and tends to zero. This process continues with the increase of k_0H, making a wavy pattern of the force. The amplitude of maximum horizontal force decreases with the increase of k_0H, vanishing at larger values of $k_0H > 11$. As the submergence depth of the block B1 increases, the k_0H values corresponding to the occurrence of minimum forces get higher (Fig. 10a). The maximum forces wane with increasing h_1/H. The horizontal force acting on block B2 is similar in nature to that on block B1. However, the horizontal force on the lower block reaches a maximum at a lower value of $k_0H = 1.15$. The effect of h_1/H is negligible on the horizontal force on block B2 (Fig. 10b). The vertical force acting on block B1 or B2 differs from the corresponding horizontal force, becoming wavier.

Figs. 12 and 13 show the horizontal and vertical forces acting on the blocks for three different gap spacing $c_1/H =$ 0.15, 0.2 and 0.25 when blocks B1 is placed at a fixed depth $h_1/H = 0.2$, with $s/H = 0.1$. The horizontal and vertical forces acting on block B1 tends to zero for $k_0H > 12$ and 15, respectively (Figs. 12(a), 13(a). However, the forces on block B2 are negligible at $k_0H \approx 8$ and onward. Figs. 12 and 13 both depict that the hydrodynamic forces vary in a wavy fashion with increasing k_0H, reaching close to zero at different values of k_0H. The zero values result from the interaction between the incident wave and reflected wave from the vertical wall. The upper block (B1) experiences a more horizontal hydrodynamic force than the lower block (B2). For the upper block, the horizontal force around the first peak shrinks with the increase in c_1/H. As does that for the lower block. The effect of c_1/H on the horizontal force of the upper block is less than that of the lower block. This is because with increasing c_1/H the lower block gets closer to the seabed. The relationship between the vertical force and c_1/H is not straight forward as that between the horizontal force and c_1/H (Fig. 12). With increasing c_1/H, the vertical force on the upper block decreases for $k_0H = 0.01 – 1.9$ but enhances for $k_0H = 1.91 – 5.34$. For the lower block, $c_1/H = 0.15$ produces the largest force for $k_0H = 0.01 – 3.2$, but beyond this limit the vertical force does not obey any particular law.

The hydrodynamic force ($|F^*_{xw}|$) acting on the vertical wall is plotted in Fig. 14 as a function of k_0H for different values of *d/H* (= 0.15, 0.25, 0.4, and 0.6), with $h_1/H = 0.2$, $h_3/H = 0.5$, and $s/H = 0.1$. The force on the vertical wall does not depend on *d/H* when $k_0H > 7.0$. There are some peaks and valleys at $k_0H = 1$-4, with peaks heightening with *d/H*. Furthermore, the peaks or valleys shift to smaller k_0H when *d/H* is increased. For example, the peak appearing at $k_0H = 2.01$ for $d/H = 0.4$ shifts to $k_0H = 1.63$ for $d/H = 0.6$. Mondal and Takagi (2019) made a similar observation in the case of a single submerged block.

The influence of incident wave angle θ on hydrodynamic force on the vertical wall is illustrated in Fig. 15. For $k_0H = 0.01 – 2.44$, the hydrodynamic force on the wall decreases with the increase in the incident angle. However, for $k_0H > 2.44$, the decrease in the force is irregular because of a strong interaction between transmitted and reflected waves. For θ = 89º, the wave is almost parallel with the vertical wall; the force on the vertical wall is therefore approximately zero.

4. Conclusions

We have formulated a boundary value problem for oblique water wave scattering by two fixed submerged blocks in the presence of a vertical step in infinite and semi-infinite domains. The problem is solved analytically using the Fourier expansion method. The velocity potentials are described explicitly in terms of infinite series solution. It is observed that for the present set of numerical values of different physical parameters, hydrodynamics forces converge for the truncated value N = 40. Therefore, this technique is more convenient than any other numerical methods (e.g. finite element method, boundary integral method) in terms of cost and computation time. We obtain the solution in explicit form. Therefore, the present results can be considered as a benchmark to compare with the result obtained from numerical techniques.

The obtained results infer that hydrodynamic horizontal and vertical forces acting on the upper block are always greater than those acting on the lower block. In the case of infinite fluid domain, the forces initially increase with k_0H and reach maxima before declining with a further increase in k_0H. On the other hand, in the case of the semi-infinite domain, when k_0H is increased, the horizontal and vertical forces vary in a damped wavy pattern. The occurrence of the wavy pattern is ascribed to the interaction between the incident and reflected waves. The horizontal force acting on the submerged bodies enhances with the increase in block thickness s/H. However, s/H has less effect on the vertical force than on the horizontal force. With the decrease of submergence depth (h_1/H), the maximum value of the horizontal force increases. The gap spacing (c_1/H) has a negligible effect on the horizontal force acting on the upper block. The force on the lower block rapidly decreases with increase c_1/H. This is attributed to the fact that the lower prism's depth increases with the increase of c_1/H. The findings are likely to be useful for the modeling of submerged bodies used as breakwater, submerged tunnel, observatories.

Acknowledgments

The authors wish to acknowledge the support given to them from National Science Foundation of China through grants 11672096 and 91752112 and from Research Grant Council of Shenzhen Government through grant JCYJ2018 0306171921088.

References

Behera, H. and Sahoo, T. (2015), "Hydroelastic analysis of gravity wave interaction with submerged horizontal flexible porous plate", *J. Fluids and Struct.*, **54**, 643-660. https://doi.org/10.1016/j.jfluidstructs.2015.01.005.

Chakrabarti, P., Chakrabarti, S.K., Olsen, T., Koo, I.S., Kim, C.W. and Huh, J.W. (2008), "Dynamic simulation of immersion of tunnel elements for Busan-Geoje fixed link project", *27th Int. Congress Ocean, Offshore Arctic Eng.*, **4**, 645-651. https://doi.org/10.1115/OMAE2008-57881.

Cheong, H.F., Shankar, N.J. and Nallayarasu, S. (1996), "Analysis of submerged platform breakwater by eigenfunction expansion method", *Ocean Eng.*, **23**(8), 649-666. https://doi.org/10.1016/0029-8018(96)84407-6.

Hu, H. Wang, K.H. and Williams, A.N. (2002), "Wave motion over a breakwater system of a horizontal plate and a vertical porous wall", *Ocean Eng.*, **29**, 373-386. https://doi.org/10.1016/S0029-8018(0r1)00029-4.

Huang, G., Zhang, N., Law, A.W.K., Song, Y. and Lin, L. (2016), "Motion response of immersing tunnel element under random waves", *Ships Offshore Struct.*, **11**(6), 561-574. https://doi.org/10.1080/17445302.2015.1038867.

Kojima, H., Yoshida, A. and Nakamura, T. (1994), "Linear and nonlinear wave forces exerted on a submerged horizontal plate", *24th Int. Congress Coastal Eng.*, https://doi.org/10.1061/9780784400890.096.

Liu, P.L.F. and Iskandarani, M. (1991), "Scattering of short-wave groups by submerged horizontal plate", *J. Waterway., Port, Coastal Ocean Eng.*, **117**(3), 235-246. https://doi.org/10.1061/(ASCE)0733-950X(1991)117:3(235).

Liu, Y., Li, Y. and Teng, B. (2009), "Wave motion over two submerged layers of horizontal thick plates", *J. Hydrodyn.*, **21**(4), 453-462. https://doi.org/10.1016/S1001-6058(08)60171-7.

Medina-Rodriguez, A. and Silva, R. (2018), "Oblique water-wave scattering by two thick submerged-horizontal plates in a two-layer fluid", *J. Waterway, Port, Coastal, Ocean Eng.*, **144**(4), 04018003. https://doi.org/10.1061/(ASCE)WW.1943-5460.0000444.

Mondal, D. and Banerjea, S. (2016), "Scattering of gravity waves by an inclined porous plate submerged in ocean with ice cover", *Q. J. Mech. Appl. Math.*, **69**(2), 195-213. https://doi.org/10.1093/qjmam/hbw004.

Mondal, R. and Takagi, K. (2016), "Wave interaction with submerged body in presence of uneven bottom", *2016 Techno Ocean*, 668-671. https://doi.org/10.1109/Techno-Ocean.2016.7890739.

Mondal, R. and Takagi, K. (2019), "Wave scattering by a fixed submerged platform over a step bottom," *Proc IMechE Part M: J Eng Maritime Env.*, **233**, 93-107.

Patarapanich, M. (1984), "Maximum and zero reflection from submerged plate", *J. Waterway., Port, Coastal Ocean Eng.*, **110**(3), 171-181. https://doi.org/10.1061/(ASCE)0733-950X(1984)110:2(171).

Patarapanich, M. and Cheong, H.F. (1989), "Reflection and transmission characteristics of regular and random waves from a submerged horizontal plates", *Coastal Eng.*, **13**, 161-182. https://doi.org/10.1016/0378-3839(89)90022-7.

Peng, W., Lee, K.H. Shin, S.H. and Mizutani, N. (2013), "Numerical simulation of interactions between water waves and inclined-moored submerged floating breakwaters," *Coast. Eng.*, **82**, 76-87. https://doi.org/10.1016/j.coastaleng.2013.07.002.

Porter, R. (2015), "Linearised water wave problems involving submerged horizontal plates", *Appl. Ocean Res.*, **50**, 91-109. https://doi.org/10.1016/j.apor.2014.07.013.

Rahman, M.A., Mizutani, N. and Kawasaki, K. (2006), "Numerical modeling of dynamic responses and mooring forces of submerged floating breakwater", *Coast. Eng.*, **53**, 799-815. https://doi.org/10.1016/j.coastaleng.2006.04.001.

Wang, K.H. and Shen, Q. (1999), "Wave motion over a group of submerged horizontal plates", *Int. J. Eng. Science*, **37**, 703-715. https://doi.org/10.1016/S0020-7225(98)00094-9.

Wang, Y., Wang, G. and Li, G. (2006), "Experimental study on the performance of the multiple-layer breakwater", Ocean Eng., **33**, 1829-1839. https://doi.org/10.1016/j.oceaneng.2005.10.017.
Williams, A.N. and McDougal, W.G. (1996), "A dynamic submerged breakwater", *J. Waterw. Port. Coast. Eng.*, **122**(6), 288-296. https://doi.org/10.1061/(ASCE)0733-950X(1996)122:6(288).
Yu, X. (2002), "Functional performance of a submerged and essentially horizontal plate for offshore wave control: a review", *Coastal Eng. J.*, **44**, 127-147. https://doi.org/10.1142/S0578563402000470.
Zheng, Y.H., Liu, P.F., Shen, Y.M., Wu, B.J. and Sheng, S.W. (2007a), "On the radiation and diffraction of linear water waves by an infinitely long rectangular structure submerged in oblique sea", *Ocean Eng.*, **34**, 436-450. https://doi.org/10.1016/j.oceaneng.2006.03.002.
Zheng, Y.H., Shen, Y.M. and Tang, J. (2007b), "Radiation and diffraction of linear water waves by an infinitely long submerged rectangular structure parallel to a vertical wall", *Ocean Eng.*, **34**, 69-82. https://doi.org/10.1016/j.oceaneng.2005.12.004.

AM